Title	Out-of-plane spin-orbit torque in polycrystalline IrMn3 for field-free perpendicular magnetization switching
Author(s)	Md Rejaul Karim, Sourabh Manna, Ayush K. Gupta, John Rex Mohan, Suman Kumar Maharana, Joseph Vimal Vas, Arnab Bose, Surbhi Gupta, Rajdeep Singh Rawat, Hironori Asada, Yasuhiro Fukuma and Rohit Medwal

Md Rejaul Karim, Manna, S., Gupta, A. K., Mohan, J. R., Maharana, S. K., Vas, J. V., Bose, A., Gupta, S., Rawat, R. S., Asada, H., Fukuma, Y., & Medwal, R. (2024). Observation of out-of-plane spin-orbit torque in a polycrystalline Py/IrMn3 heterostructure. *Physical Review B, 110*, Article 245423. https://doi.org/10.1103/physrevb.110.245423

Out-of-plane spin-orbit torque in polycrystalline $IrMn_3$ for field-free perpendicular magnetization switching

Md Rejaul Karim[1], Sourabh Manna[2], Ayush K Gupta[1], John Rex Mohan[7], Suman Kumar Maharana[1], Joseph Vimal Vas[3], Arnab Bose[4], Surbhi Gupta[5], Rajdeep Singh Rawat[2], Hironori Asada[6], Yasuhiro Fukuma[7,8] and Rohit Medwal[1*]

[1]*Department of Physics, Indian Institute of Technology Kanpur, Kanpur 208016, India*

[2]*Natural Sciences and Science Education, National Institute of Education, Nanyang Technological University 637616, Singapore*

[3]*The Ernst Ruska-Centre for Microscopy and Spectroscopy, Forschungszentrum Jülich, 52428, Germany*

[4]*Department of Electrical Engineering, Indian Institute of Technology, Kanpur, 208016 India*

[5]Department of Physics, *Motilal Nehru National Institute of Technology, Barrister Mullah Colony, Teliarganj, Prayagraj, Uttar Pradesh, 211004, India*

[6] *Department of Electronic Devices and Engineering, Graduate School of Science and Engineering, Yamaguchi University*

[7]*Department of Physics and Information Technology, Faculty of Computer Science and Systems Engineering, Kyushu Institute of Technology, 680-4 Kawazu, Iizuka 820-8502, Japan*

[8]*Research Center for Neuromorphic AI hardware, Kyushu Institute of Technology, Kitakyushu 808-0196, Japan*

[*]Correspondence should be addressed to R.M.: rmedwal@iitk.ac.in

Keywords: spin torque ferromagnetic resonance, unconventional torque, antiferromagnetic, spin Hall effect, switching, spin dynamics

ABSTRACT

The generation of on-demand out-of-plane spin polarization ($\boldsymbol{\sigma}_z$) promises an efficient field-free switching of perpendicular nano-magnet has been limited mostly in the single crystal materials. For a direct technological application, it is desired to have an out-of-plane spin current generation from polycrystalline sputtered films rather than expensive single crystalline films. Here, we report the observation of out-of-plane and in-plane torques generated by the $\hat{z}$ and $\hat{x}$ spin polarization in the polycrystalline antiferromagnet $IrMn_3$/Permalloy (Py) heterostructure. A comparatively high value of out-of-plane spin torque ratio of 0.024 has been observed with a large out-of-plane spin Hall conductivity of $\approx 2.82 \times 10^4 \, (\frac{\hbar}{2e})(\Omega m)^{-1}$. Additionally, we have investigated the underline mechanism and the fundamental role of $\hat{z}$ spins in the context of external field-free magnetization switching of a perpendicular magnetic anisotropy (PMA) material. Our findings provide a new perspective on generation and detection of out-of-plane spin polarization in antiferromagnet material and manipulate the magnetization for the development of the next generation high-density, low power consumption, logic device applications.

I. INTRODUCTION

Deterministic switching of magnetization of a perpendicular magnetic anisotropy (PMA) material is the fundamental requirement towards building low power, high speed, high-density memory solutions [1–4]. Conventional spin Hall effect (SHE) induced spin orbit torque (SOT) in ferromagnet/non-magnet (FM/NM) heterostructure can facilitate deterministic magnetization switching of a PMA material in presence of an externally applied in-plane magnetic field [cite PRL 109, 096602 (2012), 7–13]. This in-plane field breaks the rotational symmetry of magnetization switching in response to conventional SOT [5–8]. In general, the SOT comprises of an in-plane damping-like torque (DLT) given as, $\boldsymbol{\tau}_{DL,y} \propto (\boldsymbol{m} \times (\boldsymbol{\sigma} \times \boldsymbol{m})$ and an out-of-plane field-like torque (FLT) given as $\boldsymbol{\tau}_{FL} \propto \boldsymbol{\sigma} \times \boldsymbol{m}$, where $\boldsymbol{\sigma}$ is the spin polarization direction of the pure spin current generated via SHE. However, the conventional SOT-assisted deterministic magnetization switching presents two major limitations for practical device applications. Firstly, the damping-like component of the conventional SOT is inefficient in magnetization switching of a PMA material. This happens due to the symmetry of SHE-induced SOT, which is ineffective for mutually orthogonal orientation of the magnetization and the spin polarization direction [9,10]. Secondly, as stated earlier, the SOT-induced deterministic magnetization switching can be realized in presence of an in-plane symmetry breaking magnetic field. However, the external-field sources limit the scaling, consume high power, constraint by magnetic re-interference between layers, and reduce the device endurance [4,14,15]. Therefore, it is highly important to discover routes to achieve field-free deterministic magnetization switching in PMA material. Additionally, in order to generate sufficiently strong SOT to induce magnetization switching in the PMA material, a high input current (current density of the order of ~10^{12} A/m^2) is required for efficient spin current generation via SHE [5–8]. In conventional SHE, to overcome these challenges, spin source

materials with low inversion symmetry or broken magnetic mirror symmetry which are capable of generating out-of-plane ($\boldsymbol{\sigma_z}$) spin polarization can be utilized [5,16,17]. There have been several materials investigated as the efficient sources of $\boldsymbol{\sigma_z}$ such as, transition-metal dichalcogenide (TMD) [18–24], antiferromagnets (AFM) [25–29], ferromagnets (FM) [30], etc. Several methodologies have been employed to realize the external field-free and low power magnetization switching of the PMA materials such as wedge structure [31], creating lateral asymmetric structure [32], generating a tilted anisotropy using a unidirectional exchange bias in the system [33,34], by engineering a tilted anisotropy [35] and so on. However, many of these techniques are not efficient in terms of large-scale production because they require a lateral inhomogeneity which might hamper the high wafer-level study of magnetic and transport properties. Additionally, the symmetry breaking within the crystal structure to generate the unconventional out-of-plane spin-polarized spin current requires careful growth of single crystal material, which may not be feasible for large scale film production using sputtering technique. Therefore, realizing the unconventional spin current generation in polycrystalline materials are of great technological importance. On the other hand, SOTs resulting from the $\boldsymbol{\sigma_z}$ spin polarization exerts an efficient torque in the out-of-plane direction, $\boldsymbol{\tau_{DL,z} \propto m \times (\sigma_z \times m)}$ which enables the external field free and low power magnetization switching of PMA [36,37] material. This kind of magnetization switching is often referred to as unconventional SOT switching. In this regard, antiferromagnetic materials exhibiting non-trivial spin textures and strong spin-orbit coupling such as PtMn, Mn_3GaN, $IrMn_3$ have gained more attention due to their ability to generate a substantial net $\boldsymbol{\sigma_z}$ and shows the ability to switch the magnetization of PMA materials without external magnetic field.

In this work, we have demonstrated unconventional SOTs from polycrystalline sputtered $IrMn_3$ thin films along all three Cartesian axes due to the charge current flowing along $\hat{x}$ direction. The SOT has been characterized from spin torque ferromagnetic resonance (ST-FMR) experiment [cite https://doi.org/10.1103/PhysRevLett.106.036601]. The spin torque efficiency (ξ_{DL}^{z}) associated with the $\hat{z}$-polarized spins has been found to be 0.024 in a polycrystalline-IrMn3/Permalloy (NiFe or Py) bilayer. The conventional spin Hall conductivity [cite] is determined to be approximately, $\sigma_{zx}^{y} \sim 2.17 \times 10^{5}\ (\frac{\hbar}{2e})(\Omega m)^{-1}$ which is useful for minimizing the power consumption during the magnetization switching process and the out-of-plane spin Hall conductivity of $\sigma_{zx}^{z} \sim 0.28 \times 10^{5}\ (\frac{\hbar}{2e})(\Omega m)^{-1}$ which is associated with the conversion of in-plane polarized spins to out-of-plane polarized spins. Micromagnetic simulations are conducted to understand the SOT-driven magnetization dynamics and dependence of the $\hat{z}$-polarized spins observed in $IrMn_3$/Py bilayer. Additionally, we theoretically demonstrate SOT-induced deterministic magnetization switching in PMA material without any external magnetic field, by utilizing the $\hat{z}$-polarized spins. Our finding provides a route to generate the out-of-plane spin polarization in antiferromagnetic systems and its use to manipulate the magnetization direction for development of next generation high-density and power efficient memory and logic devices.

II. EXPERIMENTAL DETAILS

The sample stacks of $IrMn_3(25\ nm)$/Py $(15\ nm)/Al_2O_3(10\ nm)$ are prepared using ultra high vacuum (UHV) magnetron sputtering at room temperature. Atomically resolved high-angle annular-dark-filed (HAADF) scanning transmission electron microscopy (STEM) is employed to study the interface quality, compositional and elemental analysis of the sample. For the cross-sectional STEM measurements, the samples are prepared using a Zeiss Crossbeam focused ion

beam (FIB). In order to protect the sample from the ion beam [38], first, Pt is deposited using an electron beam. Figure 1a shows the schematic representation of the sample stacks. Cross sectional bright field images with layer thickness are shown in Fig. 1b. To understand the interlayer diffusion of the atoms and interface roughness [39], the energy dispersive X-ray spectroscopy (EDX) mapping was done. The EDX maps confirm (Figure 1c) that there is no interlayer mixing of the layers during the sample growth. Notably, at the interface of $IrMn_3$ and Py layer, a pseudo-Fe atom can be observed in the $IrMn_3$ layer because of the close atomic numbers of Fe and Mn. In order to perform the ST-FMR experiment, films are patterned into rectangular strips with dimensions of $50\ \mu m \times 20\ \mu m$ using standard photolithography and Ar-ions milling techniques. Subsequently, the GSG electrodes composed of Ti/Au are deposited and patterned onto the microstrips using dc sputtering and photolithography.

III. RESULTS AND DISCUSSION

The ST-FMR experimental setup is schematically depicted in Fig. 2a. In this set up, a microwave charge current, I_{rf} with amplitude modulation is passed through the microstrip along $\hat{x}$ which generates a transverse pure spin current ($\boldsymbol{J}_s$) along $\hat{y}$ in $IrMn_3$ via SHE (Fig. 2a). This spin current is then injected into the adjacent ferromagnetic Py layer and exerts the SOT on the local magnetization of the Py layer. The I_{rf} also induces Oersted field h_{rf} along the y-direction. Notably, the h_{rf}-induced torque on the magnetization exhibits the same effect as the field-like component of SOT. Therefore, the current-induced torques in typical FM/NM bilayers can be modelled as a sum of an in-plane DLT ($\boldsymbol{\tau}_{\parallel}$) and an out-of-plane FLT ($\boldsymbol{\tau}_{\perp}$) where the FLT includes both the field-like SOT and the Oersted field-induced torque. At the ferromagnetic resonance condition, both these torques drive the magnetization into steady state precession, resulting in the manifestation of oscillating anisotropic magnetoresistance (AMR) in the magnetic layer. Consequently, a rectified

dc voltage is generated across the sample due to the coupling of oscillatory AMR and I_{rf} [40]. A lock in amplifier is used to detect this rectified dc voltage (V_{mix}). Figure 2b shows the ST-FMR spectra of the $IrMn_3(25\ nm)/Py(15\ nm)$ sample measured while sweeping the applied in-plane magnetic field in the range of $\pm 200\ mT$ and keeping its azimuthal angle ϕ fixed at 40°. The spectra are fitted using the Lorentzian line shape function (Eq. 1) and decomposed into symmetric component (with weight factor V_S) and antisymmetric component (with weight factor V_A). The fitting equation is given below [6,41,42]:

$$V_{mix} = V_S \frac{\Delta H^2}{(H_{ext}-H_{res})^2+\Delta H^2} + V_A \frac{\Delta H(H_{ext}-H_{res})}{(H_{ext}-H_{res})^2+\Delta H^2} \quad (1)$$

where, H_{res} is the resonance field, ΔH is the linewidth measured as the half-width-half-maxima, V_S is the strength of the symmetric Lorentzian component which originates from the spin current-induced in-plane DLT and V_A is the strength of the antisymmetric Lorentzian component induced by the out-of-plane FLT [cite 10.1002/qute.202000112].. The in-plane torque $\boldsymbol{\tau}_{||}$ and out-of-plane torque $\boldsymbol{\tau}_{\perp}$ are proportional to symmetric V_S and antisymmetric component V_A respectively, which can be expressed as the following equations [19],

$$V_S = -\frac{I_{rf}}{2}\left(\frac{dR}{d\phi}\right)\frac{1}{\alpha\gamma\mu_0(2H_{res}+M_{eff})}\tau_{||} \quad (2)$$

$$V_A = -\frac{I_{rf}}{2}\left(\frac{dR}{d\phi}\right)\frac{\sqrt{1+M_{eff}/H_{res}}}{\alpha\gamma\mu_0(2H_{res}+M_{eff})}\tau_{\perp} \quad (3)$$

where, α is the Gilbert damping and γ is the gyromagnetic ratio.. The magnitude of both the DLT and FLT associated with conventional SHE is proportional to $\cos\phi$ when current is flowing along $\hat{x}$ direction and spin polarization is along $\hat{y}$ direction [43]. Therefore, if we reverse the direction of the applied magnetic field, the magnitude of V_{mix}should be same but the sign should reverse as $V_{mix}(\phi) \propto (dR/d\phi) \propto sin\,(2\phi)$ giving, $V_{mix}\,(\phi) = -V_{mix}\,(\phi + 180°)$.

In order to characterize the nature of the SOT in our $IrMn_3$/Py bilayer, we fabricate similar ST-

FMR devices from two different stacks, Pt/Py and $IrMn_3$/Py. For the Pt/Py device (Figure S8, Supporting Information), with positive and negative applied magnetic field the magnitude of symmetric and asymmetric voltage is equal with a sign reversal. But for the $IrMn_3$/Py device, the magnitude of V_S exhibits a significant disparity between positive and negative applied magnetic field, with a notably larger value observed for the positive field regime. Hence, we confirm that the SOT present in $IrMn_3$/Py system has contributions from other unconventional spin polarization in addition to the conventional spin polarization along $\hat{y}$ [44,45]. Figure 2c shows the relation between resonance field (H_r) and the frequency f which is well-fitted with the Kittel formula [46,47] [$f = \frac{\gamma \mu_0}{2\pi}\sqrt{(H_r + H_k)(H_r + H_k + M_{eff})}$], with the in-plane anisotropy field H_k, confirming that the resonance peak is solely associated with the FMR of the Py layer.

In order to get further insight on the unconventional SOT in our $IrMn_3$/Py system, we investigated the in-plane rotational symmetry of $\boldsymbol{\tau}_{||}(\propto V_S)$ and $\boldsymbol{\tau}_{\perp}(\propto V_A)$ in both $IrMn_3$/Py and Pt/Py bilayers by performing ST-FMR measurements while varying the azimuthal angle (ϕ) of the applied magnetic field. For conventional SHE-induced SOT and spin rectification effect, the resultant in-plane angular behavior of both V_S and V_A follow $sin2\phi\ cos\phi$ dependence. The absence of any anomalous SOT in this scenario can be attributed to the low magnetic moment of Pt, which is insufficient to induce the necessary magnetic asymmetry within the system which is recognized as the primary mechanism behind the generation anomalous SOT. Figure 3(a) and (b) shows the experimental angular dependence of V_S and V_A for $IrMn_3$/Py bilayer and interestingly the dependence exhibits a distinct behavior that deviates from the conventional (Pt/Py) bilayer. The dependence of three field-like and three damping like torques are given by the following equations [43,48]:

$$V_S(\phi) = S_{DL}^X \sin(2\phi)\sin(\phi) + S_{DL}^Y \sin(2\phi)\cos(\phi) + S_{FL}^Z \sin(2\phi) \quad (4)$$

$$V_A(\phi) = A_{FL}^X \sin(2\phi)\sin(\phi) + A_{FL}^Y \sin(2\phi)\cos(\phi) + A_{DL}^Z \sin(2\phi) \quad (5)$$

The constant terms can be found by fitting the ϕ-dependent ST-FMR data. The V_S obtained from the $IrMn_3$/Py sample does not fit well with conventional $sin(2\phi)\ cos(\phi)$ as the V_S has field-like torque in $\hat{z}$-direction. In addition, we observe some contribution of damping like torque from $\hat{x}$ and $\hat{y}$ spin polarization in V_S . The major contribution of antisymmetric component comes from the Oersted field generated by rf charge current in the system and the $sin(2\phi)\ cos(\phi)$ dependency implies that there is not much discontinuity in the rf distribution throughout the sample. The spin torque ratio is an important parameter which is defined as the generation of the spin torques from applied charge current density ($\boldsymbol{J}_c$) and ($\boldsymbol{J}_s$) where, $\boldsymbol{J}_s$ is the spin current being absorbed by the adjacent Py layer. The coefficient of the antisymmetric part, A_{FL}^Y is mostly due to the Oersted field [29] because of difference in the conductivity and shunting effect, we can quantify the values of the three different damping like torque ratios [29,42],

$$\xi_{DL,\,j}^X = \frac{S_{DL}^X}{A_{FL}^Y}\frac{e\mu_0 M_S t_{FM} t_{NM}}{\hbar}\sqrt{1+\frac{M_{eff}}{H_r}} \quad (6)$$

$$\xi_{DL,\,j}^Y = \frac{S_{DL}^Y}{A_{FL}^Y}\frac{e\mu_0 M_S t_{FM} t_{NM}}{\hbar}\sqrt{1+\frac{M_{eff}}{H_r}} \quad (7)$$

$$\xi_{DL,\,j}^Z = \frac{A_{DL}^Z}{A_{FL}^Y}\frac{e\mu_0 M_S t_{FM} t_{NM}}{\hbar} \quad (8)$$

where, the parameters $e, \hbar$, and M_S represent the electric charge, reduced Planck's constant, and saturation magnetization, respectively. t_{FM} and t_{NM} are the thickness of the FM and nonmagnetic layers, respectively. The term, $\xi_{DL,\,j}^Z$ does not contain the $\sqrt{1+\frac{M_{eff}}{H_r}}$ because both $A_{DL}^Z$and $A_{FL}^Y$are from the same antisymmetric component of voltage V_A. Based on this, the calculated value of the DL torques in different direction are as follows, $\xi_{DL}^y = 0.18 \pm 0.02$, and $\xi_{DL}^z = 0.024 \pm 0.05$.

The spin torque conductivity given by, $\sigma_{xz}^{\psi} = \frac{\xi_{\psi}}{\rho}\frac{\hbar}{2e}$, is defined as torques per unit area per unit electric field across the device where, ρ is the charge resistivity of the $IrMn_3$ ($\rho = 85\ \mu\Omega.cm$) and $e, \hbar$ are the charge of electron, reduced Plank's constant, respectively. We find the spin torque conductivity as, $\sigma_{zx}^{x} = -6.32 \times 10^5\ (\frac{\hbar}{2e})(\Omega m)^{-1}$, $\sigma_{zx}^{y} = 2.17 \times 10^5\ (\frac{\hbar}{2e})(\Omega m)^{-1}$, $\sigma_{zx}^{z} = 2.82 \times 10^4\ (\frac{\hbar}{2e})(\Omega m)^{-1}$. The $\hat{z}$-component of spin torque conductivity σ_{zx}^{z} is comparable with few recent reports such as, $IrMn_3$/Py [41], $MnPd_3$/CoFeB [49], Mn_3GaN/Py [50], etc. We have not observed exchange bias in our system which suggests that the unconventional torque is not associated with the exchange bias phenomenon (supplementary S5). There are few reports, where out-of-plane spin polarization has been observed in a system without any exchange coupling [25,44,45]. In our case, the presence of the unconventional torques can be considered due to the contribution arising from different polycrystalline grains of $IrMn_3$ and spin swapping effect [51]. In case of our polycrystalline samples, the orientation of grain is random and each grain can generate the spin current depending on its orientation and these contributions can add vectorially. As the contribution of each grain are not perfectly symmetrical, a net generation of $\boldsymbol{\sigma}_z$ has been observed. In $IrMn_3$/Py heterostructure, the interface also acts as a magnetic scattering center due to strong spin orbit interaction causing spin swapping effect [51,52]. This effect, where the direction of spin polarization and the direction of spin flow interchange, is facilitated by the non-collinear antiferromagnetic ordering of the $IrMn_3$ grains and its significant spin-orbit coupling. The spin swapping effect can lead to the generation of out-of-plane spin polarization, as the primary spin current is possibly generating the transverse spin polarization and secondary spin flow via spin swapping effect.

We further perform micromagnetic simulation using GPU-accelerated open source software MuMax3 [53,54] to gain a deeper understanding of the unconventional SOT and its effect on the

magnetization dynamics in the $IrMn_3$/Py system. Using Mumax3, we micromagnetically solve the LLG equation incorporating the Slonczewski-like SOT [55] given by equation (9). In non-inertial LLG equation, the magnetization dynamics is generally controlled by two factors, one is precessional torque ($\boldsymbol{\tau}_P$) which acts tangentially to the precession trajectory of the magnetization, and another is damping torque ($\boldsymbol{\tau}_D$) which tries to damp the magnetization around the effective magnetic field. After adding Slonczewski- like SOT, the dynamics of magnetization is expressed by the LLGS equation [56],

$$\frac{d\boldsymbol{m}}{dt} = -\gamma\left(\boldsymbol{m} \times \boldsymbol{H}_{eff}\right) + \alpha \boldsymbol{m} \times \frac{d\boldsymbol{m}}{dt} + \gamma \frac{\hbar}{2e} \frac{J_C(t)}{\mu_0 M_S t_{FM}} \left(\xi_{DL}^{eff}(\boldsymbol{m} \times \boldsymbol{\sigma} \times \boldsymbol{m}) + \xi_{FL}^{eff}(\boldsymbol{m} \times \boldsymbol{\sigma})\right) \quad (9)$$

where, $\boldsymbol{m}$ is the normalized magnetization vector, $\boldsymbol{H}_{eff}$ is the effective magnetic field which consists of external applied field ($\boldsymbol{H}_{ext}$), current induced Oersted field ($\boldsymbol{H}_{Oe}$), and field associated with the magnetic anisotropy in the sample ($\boldsymbol{H}_{anis}$). The third term in right hand side (RHS) represents the damping-like SOT, $\boldsymbol{\tau}_{DL}$ (i.e., the in-plane torque $\boldsymbol{\tau}_{||}$) and the last term is the field-like SOT, $\boldsymbol{\tau}_{FL}$ (i.e., the out-of-plane torque $\boldsymbol{\tau}_{\perp}$). We have considered Py dimensions as $2.560\ \mu m \times 1.60\ \mu m \times 5\ nm$ and the standard material parameters of Py such as, gyromagnetic ratio $\gamma = 29.53 \frac{GHz}{T}$, damping constant $\alpha = 0.02$, saturation magnetization $M_s = 8 \times 10^5 \frac{A}{m}$, and exchange stiffness constant $A_{ex} = 13 \times 10^{-12} \frac{J}{m}$ are used in the simulation. Here, ξ_{SH} denotes the spin Hall angle of HM, $\boldsymbol{\sigma}$ is the direction of the spin polarization and for an input charge current density $\boldsymbol{J}_c$, $\boldsymbol{J}_s$ is given as $\boldsymbol{J}_s = \xi_{SH}(\boldsymbol{J}_c \times \boldsymbol{\sigma})$. The normalized equilibrium magnetization is in the film-plane i.e., $\boldsymbol{m} = (cos\phi,\ sin\phi, 0)$. The rf current is in $\hat{x}$ direction, and the corresponding oersted field is in $\hat{y}$ direction. In a conventional SHE-SOT system, the spin polarization is taken along $\hat{y}$-direction (0,1,0) and the spin current in $\hat{z}$ direction (0,0,1). In

accordance with our experimental results, we have defined the polarization of spin in $(0.53, 0.18, 0.024)$. The magnetization dynamics are simulated with sweeping of external magnetic field H_{ext} ($\pm 100\ mT$) with a fixed applied rf frequency of 6 GHz. The time dependent magnetization data are fitted to calculate the resonance amplitude and phases. Finally, the mixing voltage of simulated ST-FMR, $V_{mix} = V_S + V_A$ are obtained from the amplitude plots for the applied magnetic field range of $\pm 100\ mT$ (Figure S7, Supporting Information). Figure 3(c) and (d) are the angle dependent plots of V_S and V_A for the case of $IrMn_3$/Py bilayer with varying the in-plane magnetic field. The simulated V_A and V_S are fitted with considering the unconventional model. The fitting clearly agrees with the experimental data indicating the presence of unconventional spin polarizations $\boldsymbol{\sigma_x}$ and $\boldsymbol{\sigma_z}$ along with the conventional $\boldsymbol{\sigma_y}$.

Achieving field-free switching of out-of-plane magnetization is crucial for dense memory applications, and this has been successfully demonstrated in antiferromagnet/ferromagnet (AFM/FM) bilayers through the exchange bias effect [10,33]. However, the exchange bias field tends to degrade as the cycling numbers increase due to Joule heating posing a challenge for its large-scale application. Presently, to ensure compatibility with CMOS techniques, a more promising solution seems to involve combining rotational angles $\boldsymbol{\sigma_y}$ and $\boldsymbol{\sigma_z}$ to achieve field-free switching in the $\hat{z}$-direction [34,57]. For our switching simulations, spin polarization's direction is chosen from the experimental data as $(0.53, 0.18, 0.024)$. Total spin Hall angle (SHA) is taken to be the 0.1, with $J_c\hat{x}$ in and J_s in $\hat{z}$ and the damping like torque ($\boldsymbol{\tau_{DL}}$) is only considered in our simulations. A FM with a strong PMA ($6 \times 10^5\ J/m^3$) is used and the initial magnetization direction is oriented along the $-\hat{z}$ direction. Figures 4(a)-(b) show the time evolution of magnetization without unconventional SOT and with unconventional SOT, respectively and in both cases a comprehensive precessional motion is observed after turning off the current pulse [57].

We performed simulations of magnetization dynamics subjected to a current pulse, characterized by a pulse width of 6 ns with rise/fall times of 5 ns as indicated by green line in Figure 4(a) and (b). In absence of unconventional $\hat{z}$ component of spin polarization, the magnetization aligns in XY plane, and no switching is observed even at the critical current density of $6 \times 10^{12}\ A/m^2$. Here, because of the non-linear dynamics of the magnetization due to low energy dissipation rate disturbs the switching phenomena (Figure 4a, c) and magnetization switches back to initial state[49] (-1). The non-reversal of magnetization switching polarity indicates that in-plane polarized spin current does not provide enough torque in the switching process of a PMA material. On the other hand, as soon as the unconventional spin polarization ($\hat{x}$, $\hat{y}$, $\hat{z}$-spins) is considered [Figure 4(b, d)], the amplitude of the precessional magnetization become large because of the cancellation of damping by $\boldsymbol{\sigma}_z$ and eventually the magnetization switches to +1 and switching of magnetization occurs. The effect of only $\hat{z}$ polarized spins on the magnetization switching dynamics has been shown in the supporting information Figure S11 where comparatively less switching time is observed with a reasonably small current density. These simulation results highlight how the unconventional SOT in our $IrMn_3$/Py system can be utilized for efficient deterministic magnetization switching of PMA materials.

IV. CONCLUSION

In conclusion, we have explored unconventional spin orbit torques in the polycrystalline $IrMn_3$/Py bilayers and its implication in the context of deterministic magnetization switching using spin torque ferromagnetic resonance experiment and micromagnetic simulations. Cross sectional STEM measurements show smooth interface without inter atomic diffusion at $IrMn_3$/Py bilayer. An out-of-plane damping like torque efficiency of 0.024 is observed indicating that even

polycrystalline $IrMn_3$ can act as an efficient out-of-plane spin polarized current source for the next generation spintronics devices. We have observed a significant in-plane spin Hall conductivity of 2.17×10^5 $(\frac{\hbar}{2e})(\Omega m)^{-1}$ and out-of-plane spin Hall conductivity of 2.82×10^4 $(\frac{\hbar}{2e})(\Omega m)^{-1}$ in $IrMn_3$. By showing good agreement between our experimental results and micromagnetic simulations, we have verified the presence of unconventional spin polarizations in the $IrMn_3$/Py system. Additionally, we have investigated the fundamental role of $\hat{z}$ polarized spins in the context of field-free magnetization switching of PMA material. These results hold immense potential for driving the field of spintronics towards new frontiers, particularly in low-power, high-speed and dense memory applications.

Data availability statement

The data that support the findings of this study are available from the corresponding author upon reasonable request.

References:

[1] A. Manchon, J. Železný, I. M. Miron, T. Jungwirth, J. Sinova, A. Thiaville, K. Garello, and P. Gambardella, *Current-Induced Spin-Orbit Torques in Ferromagnetic and Antiferromagnetic Systems*, Rev. Mod. Phys. **91**, 35004 (2019).

[2] M. I. Dyakonov and V. I. Perel, *Current-Induced Spin Orientation of Electrons in Semiconductors*, Phys. Lett. A **35**, 459 (1971).

[3] C. Song, R. Zhang, L. Liao, Y. Zhou, X. Zhou, R. Chen, Y. You, X. Chen, and F. Pan, *Spin-Orbit Torques: Materials, Mechanisms, Performances, and Potential Applications*, Prog. Mater. Sci. **118**, 100761 (2021).

[4] V. Baltz, A. Manchon, M. Tsoi, T. Moriyama, T. Ono, and Y. Tserkovnyak, *Antiferromagnetic Spintronics*, Rev. Mod. Phys. **90**, 15005 (2018).

[5] X. Xie, X. Zhao, Y. Dong, X. Qu, K. Zheng, X. Han, X. Han, Y. Fan, L. Bai, and Y. Chen, *Controllable Field-Free Switching of Perpendicular Magnetization through Bulk Spin-Orbit Torque in Symmetry-Broken Ferromagnetic Films*, Nat. Commun. **12**, 2473 (2021).

[6] L. Liu, C.-F. Pai, Y. Li, H. W. Tseng, D. C. Ralph, and R. A. Buhrman, *Spin-Torque Switching with the Giant Spin Hall Effect of Tantalum*, Science (80-.). **336**, 555 (2012).

[7] L. Liu, O. J. Lee, T. J. Gudmundsen, D. C. Ralph, and R. A. Buhrman, *Current-Induced Switching of Perpendicularly Magnetized Magnetic Layers Using Spin Torque from the Spin Hall Effect*, Phys. Rev. Lett. **109**, 96602 (2012).

[8] I. M. Miron, K. Garello, G. Gaudin, P. J. Zermatten, M. V. Costache, S. Auffret, S. Bandiera, B. Rodmacq, A. Schuhl, and P. Gambardella, *Perpendicular Switching of a Single Ferromagnetic Layer Induced by In-Plane Current Injection*, Nature **476**, 189 (2011).

[9] I. M. Miron, K. Garello, G. Gaudin, P.-J. Zermatten, M. V Costache, S. Auffret, S. Bandiera,

B. Rodmacq, A. Schuhl, and P. Gambardella, *Perpendicular Switching of a Single Ferromagnetic Layer Induced by In-Plane Current Injection*, Nature **476**, 189 (2011).

[10] S. Peng et al., *Exchange Bias Switching in an Antiferromagnet/Ferromagnet Bilayer Driven by Spin–Orbit Torque*, Nat. Electron. **3**, 757 (2020).

[11] S. Husain, N. F. Prestes, O. Fayet, S. Collin, F. Godel, E. Jacquet, T. Denneulin, R. E. Dunin-Borkowski, A. Thiaville, and M. Bibes, *Field-Free Switching of Perpendicular Magnetization in an Ultrathin Epitaxial Magnetic Insulator*, Nano Lett. (2024).

[12] N. H. D. Khang, Y. Ueda, and P. N. Hai, *A Conductive Topological Insulator with Large Spin Hall Effect for Ultralow Power Spin–Orbit Torque Switching*, Nat. Mater. **17**, 808 (2018).

[13] S. Husain, N. Figueiredo-Prestes, O. Fayet, S. Collin, F. Godel, E. Jacquet, N. Reyren, H. Jaffrès, and J.-M. George, *Origin of the Anomalous Hall Effect at the Magnetic Insulator/Heavy Metals Interface*, Appl. Phys. Lett. **122**, (2023).

[14] R. Ramaswamy, J. M. Lee, K. Cai, and H. Yang, *Recent Advances in Spin-Orbit Torques: Moving towards Device Applications*, Appl. Phys. Rev. **5**, 31107 (2018).

[15] B. Dieny, I. L. Prejbeanu, K. Garello, P. Gambardella, P. Freitas, R. Lehndorff, W. Raberg, U. Ebels, S. O. Demokritov, and J. Akerman, *Opportunities and Challenges for Spintronics in the Microelectronics Industry*, Nat. Electron. **3**, 446 (2020).

[16] H. Wu, J. Nance, S. A. Razavi, D. Lujan, B. Dai, Y. Liu, H. He, B. Cui, D. Wu, and K. Wong, *Chiral Symmetry Breaking for Deterministic Switching of Perpendicular Magnetization by Spin–Orbit Torque*, Nano Lett. **21**, 515 (2020).

[17] S. H. C. Baek, V. P. Amin, Y. W. Oh, G. Go, S. J. Lee, G. H. Lee, K. J. Kim, M. D. Stiles, B. G. Park, and K. J. Lee, *Spin Currents and Spin-Orbit Torques in Ferromagnetic Trilayers*,

Nat. Mater. **17**, 509 (2018).

[18] D. MacNeill, G. M. Stiehl, M. H. D. Guimaraes, R. A. Buhrman, J. Park, and D. C. Ralph, *Control of Spin–Orbit Torques through Crystal Symmetry in WTe2/Ferromagnet Bilayers*, Nat. Phys. **13**, 300 (2017).

[19] G. M. Stiehl, D. MacNeill, N. Sivadas, I. El Baggari, M. H. D. Guimaraes, N. D. Reynolds, L. F. Kourkoutis, C. J. Fennie, R. A. Buhrman, and D. C. Ralph, *Current-Induced Torques with Dresselhaus Symmetry Due to Resistance Anisotropy in 2D Materials*, ACS Nano **13**, 2599 (2019).

[20] Y. Liu et al., *Field-Free Switching of Perpendicular Magnetization at Room Temperature Using out-of-Plane Spins from TaIrTe4*, Nat. Electron. (2023).

[21] S. Shi et al., *All-Electric Magnetization Switching and Dzyaloshinskii–Moriya Interaction in WTe2/Ferromagnet Heterostructures*, Nat. Nanotechnol. **14**, 945 (2019).

[22] B. Zhao, B. Karpiak, D. Khokhriakov, A. Johansson, A. M. Hoque, X. Xu, Y. Jiang, I. Mertig, and S. P. Dash, *Unconventional Charge–Spin Conversion in Weyl-Semimetal WTe2*, Adv. Mater. **32**, 2000818 (2020).

[23] S. Liang, S. Shi, C.-H. Hsu, K. Cai, Y. Wang, P. He, Y. Wu, V. M. Pereira, and H. Yang, *Spin-Orbit Torque Magnetization Switching in MoTe2/Permalloy Heterostructures*, Adv. Mater. **32**, 2002799 (2020).

[24] S. Husain, R. Gupta, A. Kumar, P. Kumar, N. Behera, R. Brucas, S. Chaudhary, and P. Svedlindh, *Emergence of Spin–Orbit Torques in 2D Transition Metal Dichalcogenides: A Status Update*, Appl. Phys. Rev. **7**, (2020).

[25] J. Zhou, X. Shu, Y. Liu, X. Wang, W. Lin, S. Chen, L. Liu, Q. Xie, T. Hong, and P. Yang, *Magnetic Asymmetry Induced Anomalous Spin-Orbit Torque in IrMn*, Phys. Rev. B **101**,

184403 (2020).

[26] H. Bai, X. F. Zhou, H. W. Zhang, W. W. Kong, L. Y. Liao, X. Y. Feng, X. Z. Chen, Y. F. You, Y. J. Zhou, and L. Han, *Control of Spin-Orbit Torques through Magnetic Symmetry in Differently Oriented Noncollinear Antiferromagnetic Mn 3 Pt*, Phys. Rev. B **104**, 104401 (2021).

[27] J. Holanda, H. Saglam, V. Karakas, Z. Zang, Y. Li, R. Divan, Y. Liu, O. Ozatay, V. Novosad, and J. E. Pearson, *Magnetic Damping Modulation in IrMn 3/Ni 80 Fe 20 via the Magnetic Spin Hall Effect*, Phys. Rev. Lett. **124**, 87204 (2020).

[28] S. Hu et al., *Efficient Perpendicular Magnetization Switching by a Magnetic Spin Hall Effect in a Noncollinear Antiferromagnet*, Nat. Commun. **13**, 4447 (2022).

[29] A. Bose, N. J. Schreiber, R. Jain, D.-F. Shao, H. P. Nair, J. Sun, X. S. Zhang, D. A. Muller, E. Y. Tsymbal, and D. G. Schlom, *Tilted Spin Current Generated by the Collinear Antiferromagnet Ruthenium Dioxide*, Nat. Electron. **5**, 267 (2022).

[30] S. C. Baek, V. P. Amin, Y.-W. Oh, G. Go, S.-J. Lee, G.-H. Lee, K.-J. Kim, M. D. Stiles, B.-G. Park, and K.-J. Lee, *Spin Currents and Spin–Orbit Torques in Ferromagnetic Trilayers*, Nat. Mater. **17**, 509 (2018).

[31] S. Chen, J. Yu, Q. Xie, X. Zhang, W. Lin, L. Liu, J. Zhou, X. Shu, R. Guo, and Z. Zhang, *Free Field Electric Switching of Perpendicularly Magnetized Thin Film by Spin Current Gradient*, ACS Appl. Mater. Interfaces **11**, 30446 (2019).

[32] Y. Cao, Y. Sheng, K. W. Edmonds, Y. Ji, H. Zheng, and K. Wang, *Deterministic Magnetization Switching Using Lateral Spin–Orbit Torque*, Adv. Mater. **32**, 1907929 (2020).

[33] Y.-C. Lau, D. Betto, K. Rode, J. M. D. Coey, and P. Stamenov, *Spin–Orbit Torque Switching without an External Field Using Interlayer Exchange Coupling*, Nat. Nanotechnol. **11**, 758

(2016).

[34] S. Fukami, T. Anekawa, C. Zhang, and H. Ohno, *A Spin–Orbit Torque Switching Scheme with Collinear Magnetic Easy Axis and Current Configuration*, Nat. Nanotechnol. **11**, 621 (2016).

[35] L. You, O. Lee, D. Bhowmik, D. Labanowski, J. Hong, J. Bokor, and S. Salahuddin, *Switching of Perpendicularly Polarized Nanomagnets with Spin Orbit Torque without an External Magnetic Field by Engineering a Tilted Anisotropy*, Proc. Natl. Acad. Sci. **112**, 10310 (2015).

[36] M. Wang, J. Zhou, X. Xu, T. Zhang, Z. Zhu, Z. Guo, Y. Deng, M. Yang, K. Meng, and B. He, *Field-Free Spin-Orbit Torque Switching via out-of-Plane Spin-Polarization Induced by an Antiferromagnetic Insulator/Heavy Metal Interface*, Nat. Commun. **14**, file:///C:/Users/LENOVO/Downloads/scholar (3).ris (2023).

[37] Y. You, H. Bai, X. Feng, X. Fan, L. Han, X. Zhou, Y. Zhou, R. Zhang, T. Chen, and F. Pan, *Cluster Magnetic Octupole Induced Out-of-Plane Spin Polarization in Antiperovskite Antiferromagnet*, Nat. Commun. **12**, 6524 (2021).

[38] R. Medwal, A. Deka, J. V. Vas, M. Duchamp, H. Asada, S. Gupta, Y. Fukuma, and R. S. Rawat, *Facet Controlled Anisotropic Magnons in Y3Fe5O12 Thin Films*, Appl. Phys. Lett. **119**, 162403 (2021).

[39] N. Manikanthababu, C. Joishi, J. Biswas, K. Prajna, K. Asokan, J. V Vas, R. Medwal, R. C. Meena, S. Lodha, and R. Singh, *Ion Irradiation-Induced Interface Mixing and the Charge Trap Profiles Investigated by In Situ Electrical Measurements in Pt/Al $ _ {\text {2}} $ O $ _ {\text {3}} $/$\beta $-Ga $ _ {\text {2}} $ O $ _ {\text {3}} $ MOSCAPs*, IEEE Trans. Electron Devices (2023).

[40] M. Harder, Y. Gui, and C.-M. Hu, *Electrical Detection of Magnetization Dynamics via Spin Rectification Effects*, Phys. Rep. **661**, 1 (2016).

[41] W. Zhang, W. Han, S.-H. Yang, Y. Sun, Y. Zhang, B. Yan, and S. S. P. Parkin, *Giant Facet-Dependent Spin-Orbit Torque and Spin Hall Conductivity in the Triangular Antiferromagnet IrMn3*, Sci. Adv. **2**, e1600759 (2016).

[42] L. Liu, T. Moriyama, D. C. Ralph, and R. A. Buhrman, *Spin-Torque Ferromagnetic Resonance Induced by the Spin Hall Effect*, Phys. Rev. Lett. **106**, 36601 (2011).

[43] J. Zhou et al., *Magnetic Asymmetry Induced Anomalous Spin-Orbit Torque in IrMn*, Phys. Rev. B **101**, 184403 (2020).

[44] S. Liang, L. Han, Y. You, H. Bai, F. Pan, and C. Song, *Interface-Relevant out-of-Plane Spin Polarization in Ir Mn 3/Permalloy Bilayers*, Phys. Rev. B **107**, 184427 (2023).

[45] A. Kumar, P. Gupta, N. Chowdhury, K. I. A. Khan, U. Shashank, S. Gupta, Y. Fukuma, S. Chaudhary, and P. K. Muduli, *Interfacial Origin of Unconventional Spin-Orbit Torque in Py/Γ− γ- IrMn3*, Adv. Quantum Technol. 2300092 (2023).

[46] C. Kittel and P. McEuen, *Introduction to Solid State Physics, Vol 8 Wiley New York*, (1976).

[47] M. R. Karim, A. Adhikari, S. N. Panda, P. Sharangi, S. Kayal, G. Manna, P. S. A. Kumar, S. Bedanta, A. Barman, and I. Sarkar, *Ultrafast Spin Dynamics of Electrochemically Grown Heusler Alloy Films*, J. Phys. Chem. C **125**, 10483 (2021).

[48] W. L. Yang, J. W. Wei, C. H. Wan, Y. W. Xing, Z. R. Yan, X. Wang, C. Fang, C. Y. Guo, G. Q. Yu, and X. F. Han, *Determining Spin-Torque Efficiency in Ferromagnetic Metals via Spin-Torque Ferromagnetic Resonance*, Phys. Rev. B **101**, 1 (2020).

[49] M. Dc, D.-F. Shao, V. D.-H. Hou, A. Vailionis, P. Quarterman, A. Habiboglu, M. B. Venuti, F. Xue, Y.-L. Huang, and C.-M. Lee, *Observation of Anti-Damping Spin–Orbit Torques*

Generated by in-Plane and out-of-Plane Spin Polarizations in MnPd3, Nat. Mater. 1 (2023).

[50] T. Nan et al., *Controlling Spin Current Polarization through Non-Collinear Antiferromagnetism*, Nat. Commun. **11**, (2020).

[51] M. B. Lifshits and M. I. Dyakonov, *Swapping Spin Currents: Interchanging Spin and Flow Directions*, Phys. Rev. Lett. **103**, 186601 (2009).

[52] B. K. Hazra et al., *Generation of Out-of-Plane Polarized Spin Current by Spin Swapping*, Nat. Commun. **14**, 4549 (2023).

[53] A. Vansteenkiste, J. Leliaert, M. Dvornik, M. Helsen, F. Garcia-Sanchez, and B. Van Waeyenberge, *The Design and Verification of MuMax3*, AIP Adv. **4**, 107133 (2014).

[54] J.-W. Xu and A. D. Kent, *Charge-to-Spin Conversion Efficiency in Ferromagnetic Nanowires by Spin Torque Ferromagnetic Resonance: Reconciling Lineshape and Linewidth Analysis Methods*, Phys. Rev. Appl. **14**, 14012 (2020).

[55] J. C. Slonczewski, *Current-Driven Excitation of Magnetic Multilayers*, J. Magn. Magn. Mater. **159**, L1 (1996).

[56] J. Park, G. E. Rowlands, O. J. Lee, D. C. Ralph, and R. A. Buhrman, *Macrospin Modeling of Sub-Ns Pulse Switching of Perpendicularly Magnetized Free Layer via Spin-Orbit Torques for Cryogenic Memory Applications*, Appl. Phys. Lett. **105**, (2014).

[57] K.-S. Lee, S.-W. Lee, B.-C. Min, and K.-J. Lee, *Threshold Current for Switching of a Perpendicular Magnetic Layer Induced by Spin Hall Effect*, Appl. Phys. Lett. **102**, (2013).

Figure Captions:

Figure 1. Microstructures and elemental analysis of the sample: (a) A schematic representation of the $IrMn_3$/NiFe/AlO heterostructures illustrates the layer structure of the device, where AlO layer on top acting as a capping layer. (b) High magnification HAADF-STEM image at the interface of $IrMn_3$/NiFe interface. The atomic columns of both $IrMn_3$ and NiFe are distinctly observed due to the z-contrast imaging mode where heavier elements appear brighter. This image also provides the thickness of each layer of the entire stack. (c) HAADF-STEM image with energy dispersive x-ray (EDS) spectroscopy compositional mapping of the elements such as Ir, Mn, Ni, Fe, and Al at and near the interface.

Figure 2. ST-FMR measurement setup: (a) The typical ST-FMR schematic setup and measurement geometry of $IrMn_3$/NiFe with bias-tee. This figure also illustrated the main component of the device and the direction of the different torques acting on the adjacent NiFe layer. (b) Lorentzian fitting of the mixing voltage at 6 GHz for positive and negative applied magnetic field. V_{Sym} represents the symmetric component of the signal and V_{Asym} represents the antisymmetric part of the signal. (c). Kittel fit from frequency range 4 to 7 GHz at φ=40° and the corresponding M_{eff}.

Figure 3. Angle dependent ST-FMR measurements: (a, b) Extracted components of $IrMn_3$/Py sample for 6 GHz rf frequency at 40º (a) Symmetric contribution V_S as function of in-plane angle of applied magnetic field (ϕ_H) and the fitted parameters. (b) components of the Antisymmetric contribution V_A. (c), (d) The schematic of an unconventional SOT system with spin polarization in three axes (c) The Symmetric components of simulated data (d) Antisymmetric components of the simulated data.

Figure 4. Current induced magnetization switching from mumax simulation: (a) The time evolution of the components of magnetization (M_x, M_y, M_z) without $\boldsymbol{\sigma_z}$ (in absence of the external magnetic field) (b) This figure depicts the magnetization switching dynamics induced by current pulses in the presence of $\boldsymbol{\sigma_x}, \boldsymbol{\sigma_y}, \boldsymbol{\sigma_z}$ (c) The snapshots of switching trajectories of the magnetization without $\boldsymbol{\sigma_z}$. (d) Snapshots of magnetization switching dynamics induced by current pulses in presence of $\boldsymbol{\sigma_x}, \boldsymbol{\sigma_y}, \boldsymbol{\sigma_z}$.

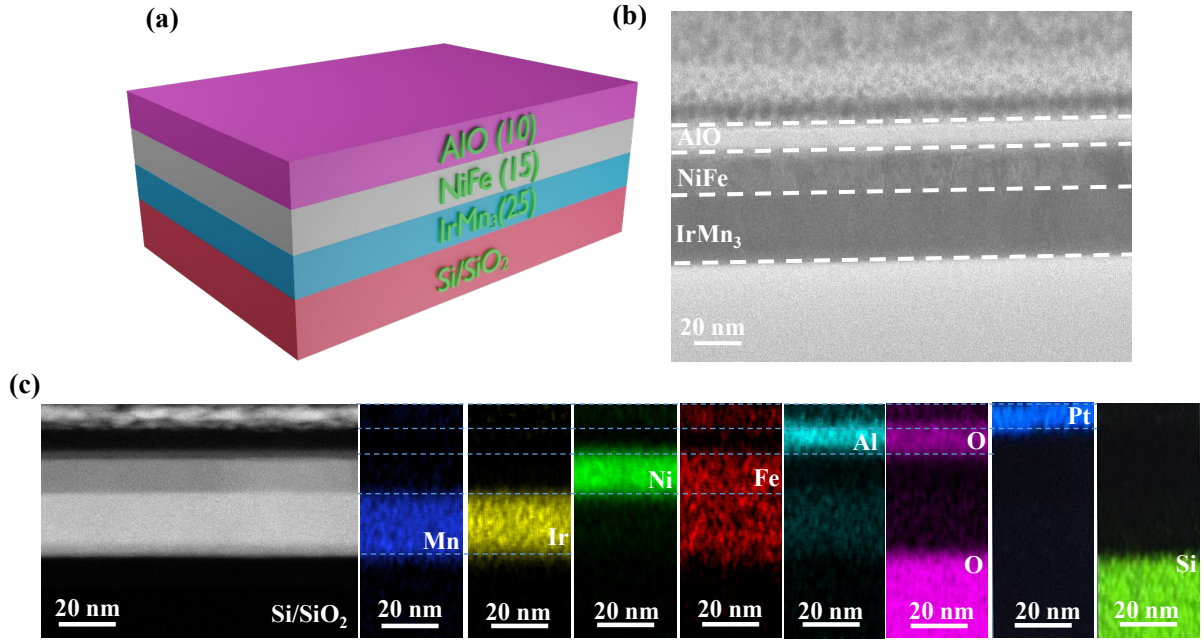

Figure 1. Microstructures and elemental analysis of the bilayer

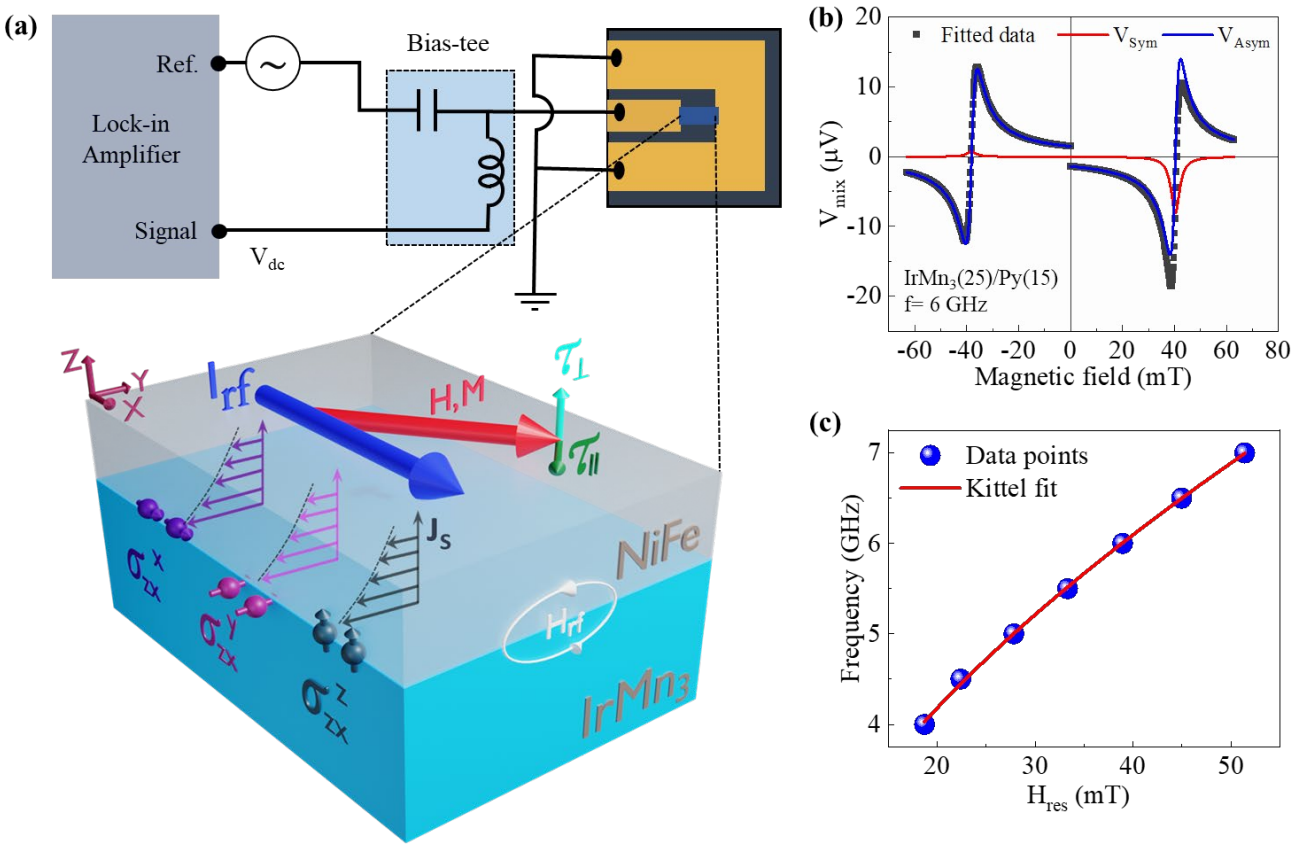

Figure 2. Schematic of a ST-FMR setup

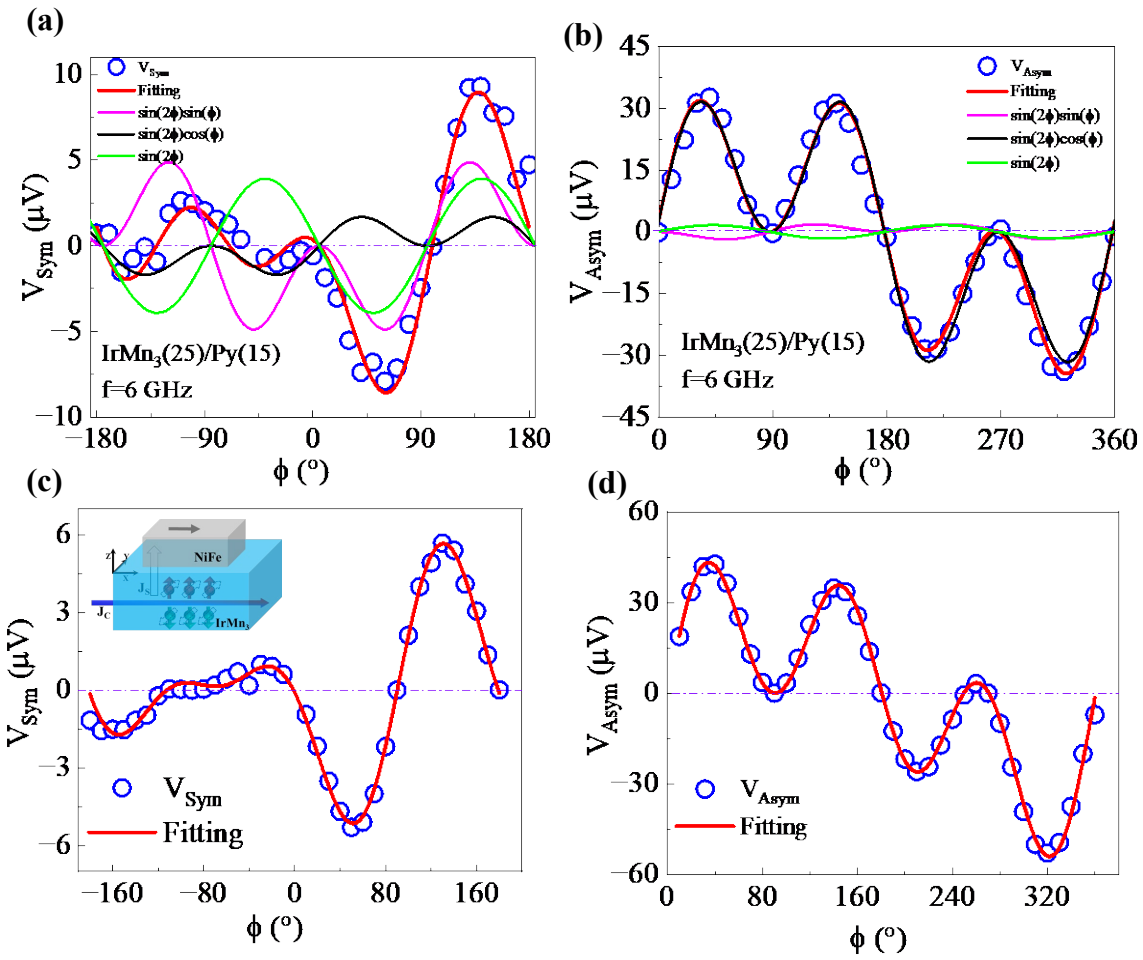

Figure 3. Experimental and simulated angular dependence data $IrMn_3$/Py bilayers.

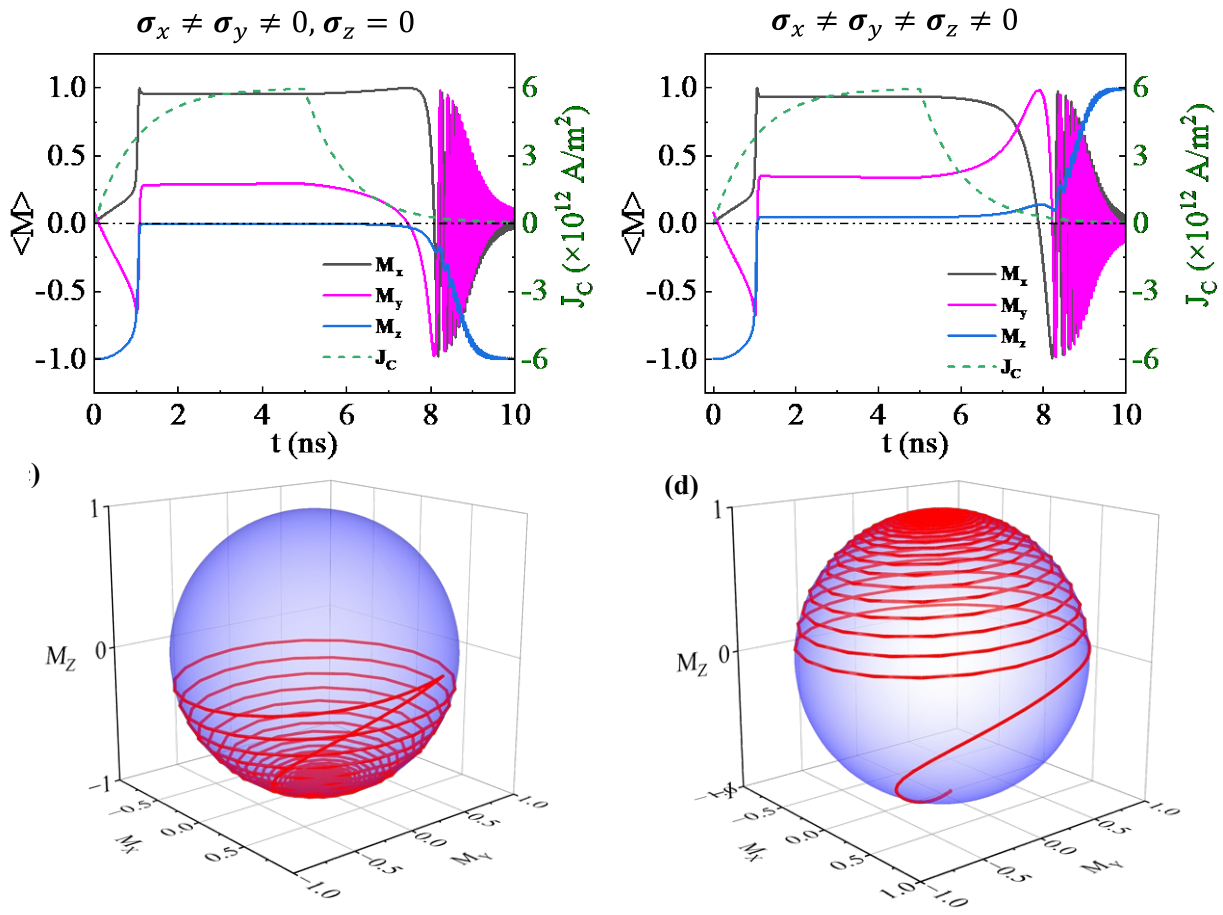

Figure 4. Magnetization switching in MuMax3 simulation without $\boldsymbol{\sigma_z}$ and with $\boldsymbol{\sigma_x}, \boldsymbol{\sigma_y}, \boldsymbol{\sigma_z}$.

Table I. Summary of the different spin torque efficiencies measured at room temperature reported so far:

Materials	ρ (μΩ·cm)	ξ_{DL}^{x}	ξ_{DL}^{y}	ξ_{DL}^{z}	Ref.
$IrMn_3$	85	-	0.18	0.024	This work
WTe_2	380	-	0.03	0.013	Ref. 18
Mn_3GaN	225	-0.013	0.025	0.019	Ref. 50
Mn_3SnN	-	-	-	0.003	Ref. 37
$MnPd_3$	60	-	0.41	0.011	Ref. 49